PAPER

Naphthalene diimide-based random terpolymer acceptors for constructing all-polymer solar cells with enhanced fill factors†

Baitian He, [ID] *[a] Longfei Liu, [ID] [b] Yan Liu,[a] Guiting Chen, [ID] *[a] Manjun Xiao*[b] and Chuanbo Dai[a]

All-polymer solar cells (all-PSCs) with mechanical and thermal stability have potential for applications in flexible devices. Polymer acceptors based on naphthalene diimide (NDI) have been widely studied because of their strong electron affinity, high electron mobility, and high mechanical reliability. However, controlling the film morphology of the polymer–polymer blends of NDI-based all-PSCs is difficult. Consequently, all-PSCs based on NDI building blocks exhibit a low fill factor (FF) and a lower power-conversion efficiency (PCE) than state-of-the-art polymer solar cells. In this work, we added a small amount of dicyanodistyrylbenzene (DCB) unit to the NDI-based polymer acceptor N2200 through random copolymerization and synthesized a series of NDI-based terpolymer acceptors PNDI*x*, where *x* is the molar concentration of DCB units relative to NDI units. PNDI5 and PNDI10, corresponding to 5% and 10% molar concentrations of DCB, respectively, showed lower crystallization and good miscibility with PBDB-T, a widely used electron-donating copolymer, than the terpolymer based on DCB-free N2200. Moreover, compared to the PBDB-T:N2200 device, the PNDI5-based device exhibited a much higher PCE (8.01%), and an enhanced FF of 0.75 in all-PSCs. These results indicate that ternary random copolymerization is a convenient and effective strategy for optimizing the film morphology of NDI-based polymers, and that the resulting terpolymer acceptor is a promising n-type acceptor for constructing high-performance all-PSCs.

[a]*School of Chemistry and Environment, Jiaying University, Meizhou 514015, P. R. China. E-mail: baitian-he@foxmail.com; 576146400@qq.com*

[b]*College of Chemistry, Key Lab of Environment-Friendly Chemistry and Application, (Ministry of Education), Xiangtan University, Xiangtan 411105, P. R. China. E-mail: xmj0704@163.com*

† Electronic supplementary information (ESI) available: additional figures as mentioned in the text, including synthesis of monomer and polymer, and device fabrication and characterizations. See https://doi.org/10.1039/d2ra03062d

Introduction

All-polymer solar cells (all-PSCs), composed of a polymeric electron donor and a polymeric electron acceptor, display morphological stability and flexibility.[1–4] Thus, they have gained increasing attention and were being considered for commercial applications.[5–7] However, the entanglement of polymer chains in polymer–polymer blends disfavors the formation of a phase-separated morphology that can facilitate charge separation and transportation.[8–12] Consequently, the overall photovoltaic performances of current all-PSCs are less than those of devices based on small-molecule acceptors. Much effort has been devoted to developing highly efficient polymer acceptors, which are mainly constructed from several electron deficient fragments, such as naphthalene diimide (NDI),[13–16] perylene

diimide (PDI),[17,18] B ← N bridged bipyridine (BNBP),[19,20] a fused-ring electron acceptor (FREA),[21–23] bithiophene imide (BTI).[6,24] Recently, a series of new polymer acceptors with high light-absorption capacity had been constructed from Y6, a small-molecule building block. These acceptors can increase the power conversion efficiency (PCE) of all-PSCs to 15%.[25–29]

NDI-based acceptors, especially poly[[*N,N*′-bis(2-octyldo-decyl)-naphthalene-1,4,5,8-bis(dicarboximide)-2,6-diyl-*alt*]-5,5′-(2,2′-bithiophene)] (N2200), were candidate polymer acceptors for manufacturing commercial all-PSCs, owing to their ease of synthesis, strong electron affinities, high electron mobilities, and high mechanical reliabilities.[30] However, N2200 exhibited strong crystalline and poor miscibility with polymer donors, resulting in large crystalline domains between polymer donor and polymer acceptor, which leads to suboptimal morphology and retard the performance of all-PSCs.[31,32] Consequently, only several collocations could offer a PCE over 8%. Pre-aggregating donor and acceptor polymers in 2-methyl tetrahydrofuran, processing active layers with an environmentally friendly solvent, and preparing active layers *via* slot-die coating could help mitigate the problems associated with N2200.[12,13,33] More-over, several research groups have modified the molecular architecture of N2200 to control the crystallinity of NDI-based polymer acceptors. These researchers incorporated another

donor or acceptor unit to construct N2200 derivatives with a D_1–A–D_2–A or D–A_1–D–A_2 structure. For example, Jenekhe *et al.*,[14] Wang *et al.*,[34] Huang *et al.*,[35] Chen *et al.*,[36] and Kim *et al.*[37] had optimized the molecular structures of NDI-based polymers through a terpolymerization strategy. Therefore, random copolymerization is a potential technique for fine-tuning the crystallinity of NDI-based polymer acceptors to effectively control film morphology.

In this study, we incorporated a small amount of dicyanodistyrylbenzene (DCB) unit into N2200 through random polymerization to control the molecular topology of N2200 and generate a series of new terpolymer acceptors. The synthesized terpolymer acceptors are denoted as PNDI5 and PNDI10, as they contained 5% and 10% molar concentrations of DCB, respectively (Scheme 1). Previous research had reported that introducing cyanovinylene into photoactive materials can control polymer crystallization and promote exciton dissociation and electron transport.[38,39] We found that the terpolymer acceptor crystallization temperature (T_c) gradually decreased with increasing DCB concentration, as this led to a decrease in the rigidity of the molecular backbone and in intermolecular stacking.[20] Compared with PNDI10-based devices, devices based on the PNDI5 and a PBDB-T (poly[[2,6-(4,8-bis(5-(2-ethylhexyl)thiophen-2-yl)-benzo[1,2-*b*:4,5-*b*]dithiophene))-*alt*-(5,5-(1,3-di-2-thienyl-5,7-bis(2-ethylhexyl)benzo[1,2-*c*:4,5-*c*]dithiophene-4,8-dione)])]) donor exhibited more favorable film morphologies, more balanced hole/electron mobilities, and lower bimolecular recombination, leading to enhanced PCE of up to 8.01% with a higher J_{sc} of 12.9 mA cm^{-2} and fill factor (FF) of 0.75. These results demonstrate that random copolymerization, which changes the molecular structures of NDI-based polymer acceptors, is an effective strategy for manufacturing all-PSCs with favorable morphologies and enhanced efficiencies.

Results and discussion

A series of NDI-based terpolymer acceptors was synthesized *via* Stille polymerization of bistannylated bithiophene (Th$_2$-SnMe$_3$), dibromo-NDI (NDI-Br$_2$), and a (2E, 2′E)-3,3′-(2,5-bis(2-ethylhexyloxy)-1,4-phenylene)bis(2-(5-(trimethylstannyl)thiophen-2-yl)acrylonitrile) (DCB-SnMe$_3$) as the starting materials. The synthetic route and detailed procedures for the preparation of the copolymers are described in the ESI (Fig. S1†). The synthesized terpolymer acceptors (PNDI5 and PNDI10) were dissolved in common organic solvents, such as toluene, chloroform, and chlorobenzene, or transformed into uniform films by spin-casting. The average molecular weights of the copolymers were determined *via* high-temperature gel permeation chromatography in 1,2,4-trichlorobenzene, with respect to a polystyrene standard (Table 1). The number-average molecular weights of N2200, PNDI5, and PNDI10 were 75.7, 68.5, and 60.6 kDa, with polydispersity indices of 1.83, 1.85, and 1.93, respectively.

The thermal properties of the polymer acceptors were evaluated *via* differential scanning calorimetry (Fig. 1). The melting temperatures (T_m) and crystallization temperatures (T_c) of the PNDI5 (321 °C and 298 °C) and PNDI10 (316 °C and 286 °C) copolymers were less than those of N2200 (328 °C and 307 °C, respectively). The reduction in T_m and T_c is attributable to the reduced intermolecular stacking of the copolymers owing to the increased backbone disorder.[32] Thermogravimetric analysis (TGA) (Fig. S6, ESI†) shows that the onset decomposition temperatures of the copolymers with 5% weight loss (T_d) were 380.6 °C, 454.8 °C, 435.4 °C and 420.7 °C for PBDB-T, N2200, PNDI5 and PNDI10, respectively, indicating good thermal stability of the copolymers.
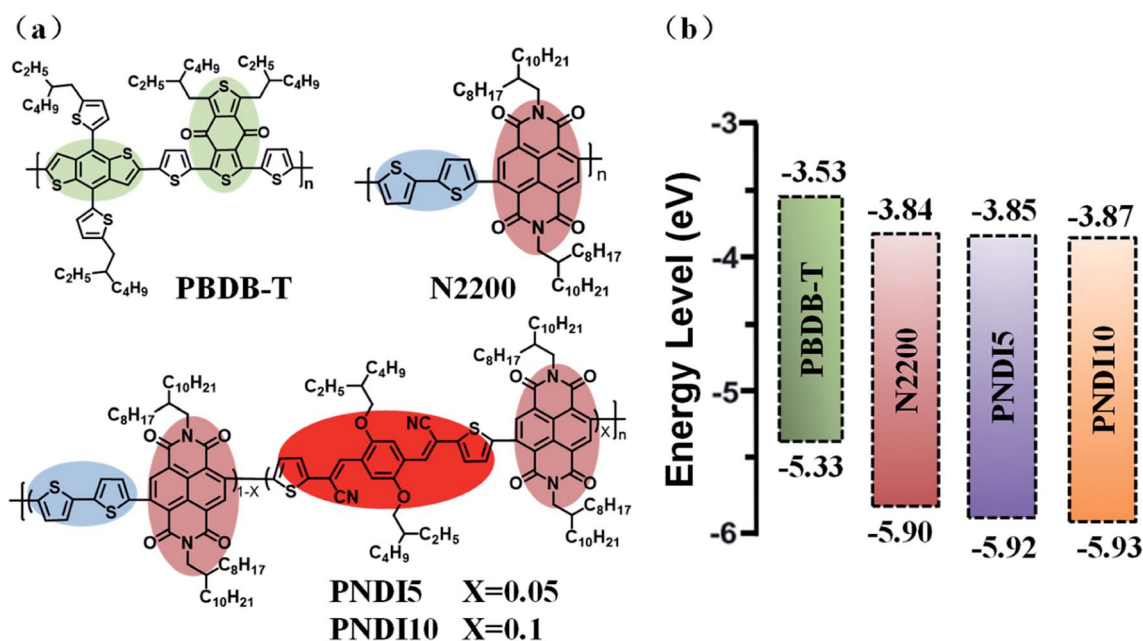
Scheme 1 (a) Molecular structures of polymer donor and terpolymer acceptors; (b) energy levels of PBDB-T, PNDI5, PNDI10 and N2200.

Table 1 Molecular weight, absorption, electrochemical properties, and thermal transition for copolymers

Copolymers	M_n^a (kDa)	PDI^a	λ_{max}^{sol} (nm)	λ_{max}^{film} (nm)	HOMO^b (eV)	LUMO^b (eV)	E_g^{cv} (eV)	T_m (°C)	T_C (°C)
N2200	75.7	1.83	706	718	−5.90	−3.84	2.06	304	326
PNDI5	68.5	1.85	675	696	−5.92	−3.85	2.07	292	313
PNDI10	60.6	1.93	645	688	−5.93	−3.87	2.06	284	305

^{a} Determined by gel permeation chromatography (1,2,4-trichlorobenzene) against PS standards. ^{b} Measured by cyclic voltammetry.
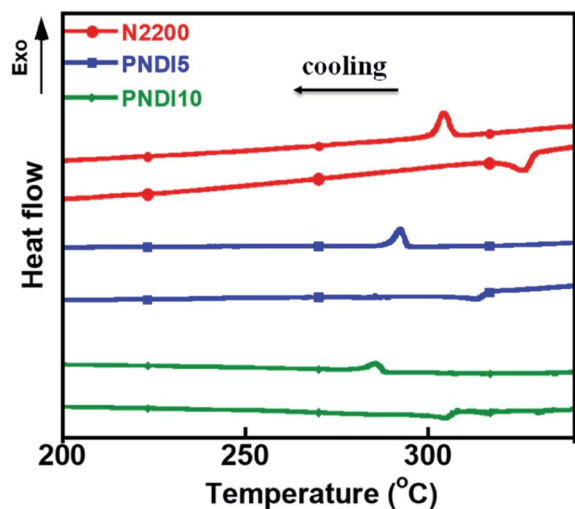

Fig. 1 Differential scanning calorimetric characteristics of N2200, PNDI5, and PNDI10. The measurement was performed at a heating/cooling rate of 10 °C min^{-1} under nitrogen.

Optical and electrochemical properties

The normalized ultraviolet-visible absorption spectra of the polymer acceptors (N2200, PNDI5, PNDI10), both in chloroform solution and as thin films, are shown in Fig. 2, and the detailed parameters are listed in Table 1. The spectra of all of the polymer acceptors in solution showed two absorption bands characteristic to donor–acceptor conjugated polymers: a short-wavelength absorption band at approximately 370 nm,

attributed to the π–π* transition of the main chain, and a low-energy band (500–800 nm), attributed to the intra-molecular charge-transfer effect. The low-energy band of the terpolymer acceptor exhibited a hypsochromic shift, due to the backbone planarity of the polymer being lower than that of N2200.[40] The spectra of the thin-film polymer acceptors showed red-shifted absorption peaks, which indicated the effective stacking of polymer chains in the solid state. Moreover, the PNDI5 and PNDI10 polymer acceptors exhibited complementary absorption with the PBDB-T donor.

The highest occupied molecular orbital (HOMO) and lowest unoccupied molecular orbital (LUMO) levels of polymer acceptors were measured by cyclic voltammetry (CV) (Fig. S7, ESI†), and the detailed parameters are listed in Table 1. The synthesized terpolymer acceptors exhibited identical HOMO energy levels (−5.9 eV). Owing to the effect of the DCB unit, the LUMO of the acceptor polymers were slightly less than that of the reference polymer (N2200), which may be related to electron withdrawal from the polymer backbone.[22]

Photovoltaic properties

Bulk heterojunction all-PSCs were fabricated to evaluate the photovoltaic properties of the synthesized terpolymer acceptors, which had the conventional configuration of ITO/PEDOT:PSS/PBDB-T:acceptor/PFN-Br/Al. A thin layer (∼5 nm) of water-/alcohol-soluble poly[(9,9-bis(3-((N,N-dimethyl)-N-ethylammonium)propyl)-2,7-fluorene)-alt-2,7-(9,9-dioctylfluorene)] dibromide (PFN-Br) was used as the cathode interlayer because it can facilitate electron collection through the formation of an
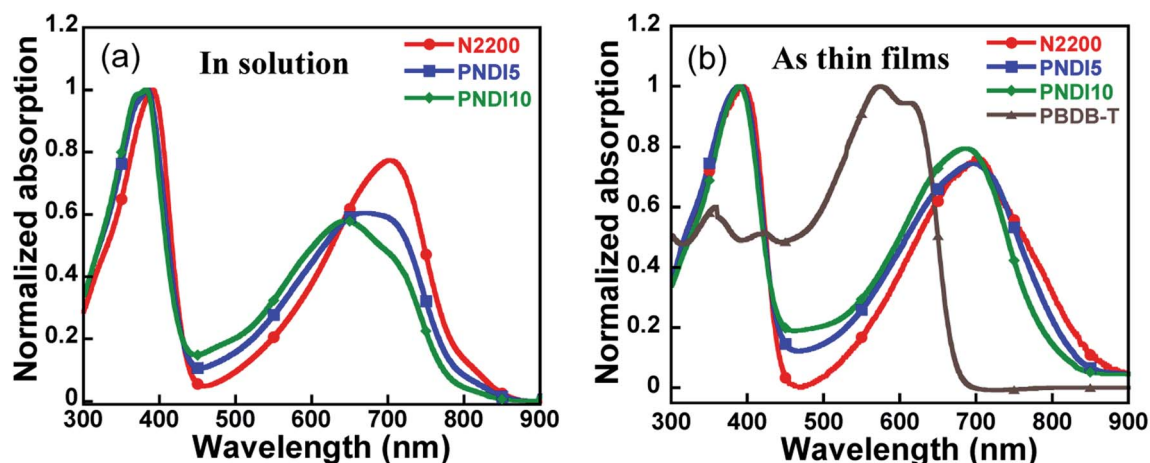

Fig. 2 Normalized UV-vis absorption spectra of copolymers in chloroform solutions (a) and as thin films (b).
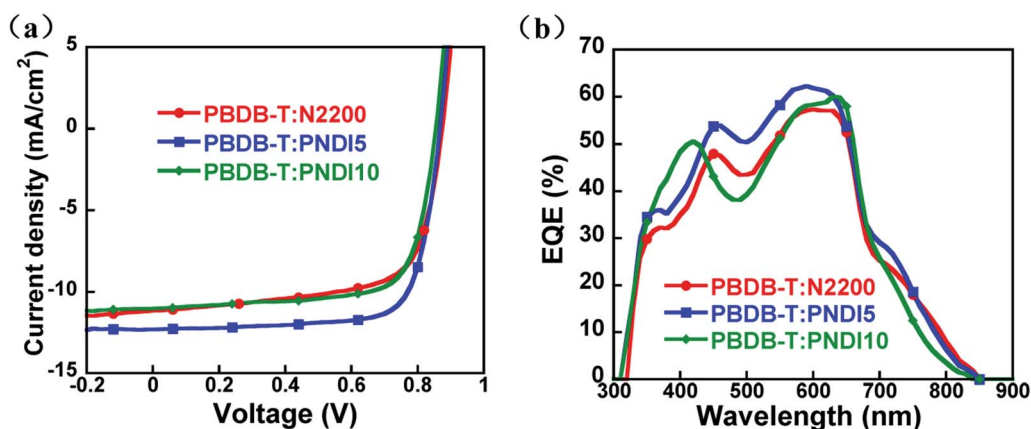
Fig. 3 (a) J–V characteristics and (b) EQE spectra of devices with photoactive layer of PBDB-T:acceptor (1 : 0.5, wt : wt).

interfacial dipole.[41] To obtain the optimal photovoltaic performances, the device based on PBDB-T:PNDI5 was initially chose to optimize processing condition from the donor-to-acceptor weight ratios, thermal annealing temperatures, volume of additive, and thickness of the active layer. The data are detailed in ESI (Table S1–S4†). The current density–voltage (J–V) curves and external quantum efficiency (EQE) spectra of the optimized devices are shown in Fig. 3, and the relevant photovoltaic parameters are summarized in Table 2.

All of the devices showed the similar open-circuit voltage (V_{oc}). The device based on PBDB-T-N2200 (control device) showed a PCE of 6.60% (J_{sc} = 11.00 mA cm^{-2}, FF = 67.22%), consistent with previous results reported for a similar active layer.[42] The PNDI5-based device considerably outperformed the control device by achieving a PCE of 8.01% (J_{sc} = 12.32 mA cm^{-2}; FF = 74.94%). The higher FF of the PNDI5-based device was due to its balanced hole/electron mobilities and more homogeneous morphology than the control device. Moreover, compared with the PNDI5-based device, the PNDI10-based device, with a higher DCB loading, exhibited a slightly lower PCE (6.81%; J_{sc} = 10.93 mA cm^{-2}; FF = 72.00%), because of its disordered molecular packing and unfavorable blend morphology.[36]

The EQE spectral of the devices are shown in Fig. 3b. All blend films showed a broad photocurrent response from 300 to 850 nm, consistent with their absorption spectra. This indicates that both the polymer acceptor and PBDB-T polymer donor in the blend films exhibited a photocurrent. Devices based on PBDB-T-PNDI5 showed better spectral responses at 350–750 nm than the N2200-based device, which is consistent with the higher J_{sc} of the former devices. The enhanced J_{sc} values of the

devices based on a random polymer acceptor correlated well with the changes in their EQE spectral responses.

Charge generation, transport properties and recombination

To reveal the exciton dissociation and charge collection processes of the all-PSCs based on a PBDB-T:acceptor, we investigated the dependence of the photocurrent density (J_{ph}, $J_{ph} = J_L - J_D$, where J_L and J_D are the light and dark current densities, respectively) on the effective voltage (V_{eff}, $V_{eff} = V_0 - V_{bias}$, where V_0 is the voltage when J_{ph} is 0 and V_{bias} is the applied bias voltage.) at an illumination of 100 mW cm^{-2},[43,44] and the relevant characteristics are shown in Fig. 4a. We presume that at a high V_{eff} (>2 V), all photogenerated excitons were dissociated into free charges and collected by electrodes, and the J_{ph} reaches saturation (J_{sat}). Thus, the maximum exciton generation rates ($G_{max} = J_{sat}/qL$), where J_{sat} is the saturated photocurrent density, q is the electronic charge, and L is the thickness of the active layer of devices, are summarized in Table S5.† The PNDI5-based devices presented slightly higher G_{max} values (7.93 × 10^{27}) than the N2200-based devices (7.43 × 10^{27}), which indicates that the PNDI5-based device generated excitons faster than N2200 counterparts, consistent with the J_{sc} values. In addition, the charge-dissociation probability $P(E, T)$ was determined by normalizing J_{ph} with J_{sat}. Under short-circuit conditions, the $P(E, T)$ values the N2200- and PNDI5-based devices were 91.60% and 94.49%, respectively. These results indicate that the PNDI5-based device exhibited better exciton dissociation rates and more efficient charge collection than the N2200-based device.

Table 2 Photovoltaic parameters of the optimized PBDB-T:acceptor and mobility of blend films

Active layer[a]	V_{oc} (V)	J_{sc} (mA cm^{-2})	J_{sc}, EQE[c] (mA cm^{-2})	FF (%)	PCE[b] (max) (%)
PBDB-T:N2200	0.87 ± 0.01	11.00 ± 0.13	10.78	67.22 ± 0.53	6.45 ± 0.10 (6.55)
PBDB-T: PNDI5	0.87 ± 0.01	12.32 ± 0.01	11.80	74.94 ± 0.02	8.01 ± 0.01 (8.02)
PBDB-T: PNDI10	0.86 ± 0.01	10.93 ± 0.19	10.65	72.00 ± 0.49	6.70 ± 0.12 (6.82)

[a] D : A = 1 : 0.5; all blend films were processed by chlorobenzene with 0.5 vol% DIO. [b] Best PCE values are obtained from 12 separate devices. [c] Obtained from the integration of EQE spectra.
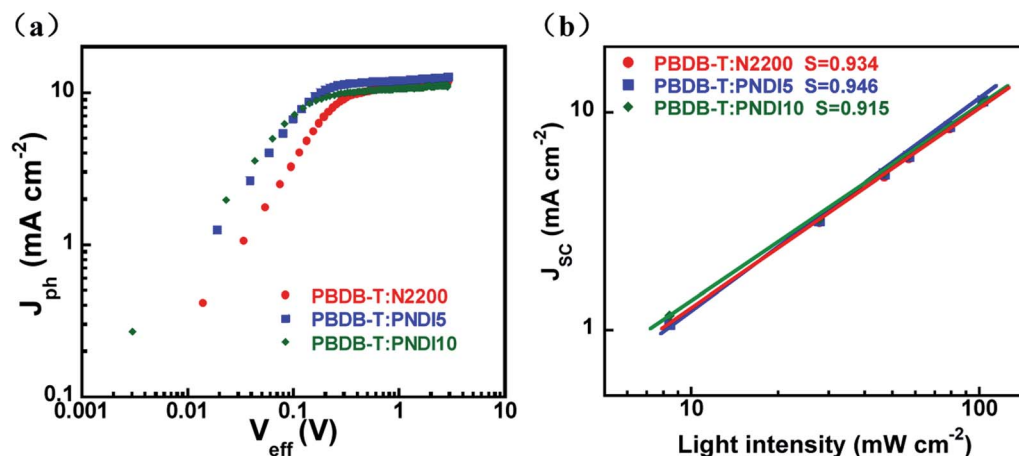
Fig. 4 (a) $J_{ph}-V_{eff}$ and (b) J_{SC} as a function of light intensity.

Table 3 Carrier mobilities of PBDB-T:Acceptor devices

PBDB-T:Acceptor	μ_h (cm^2 V^{-1} s^{-1})	μ_e (cm^2 V^{-1} s^{-1})	μ_h/μ_e
N2200	1.52×10^{-3}	4.01×10^{-5}	38
PNDI5	1.00×10^{-3}	2.85×10^{-4}	3.5
PNDI10	1.80×10^{-3}	3.08×10^{-4}	5.8

In addition, the charge transport properties of blended films were evaluated *via* the space–charge-limited current method. The corresponding *J–V* characteristics are shown in Fig. S3 (ESI†), and the carrier mobility is summarized in Table 3. The hole/electron mobility balances (μ_h/μ_e), which depended on the DCB molar concentration, exhibited nonmonotonic behaviors. A balanced carrier mobility is a crucial factor affecting the FF of all-PSCs. Among all of the blends, the PNDI5-based blend film showed the most balanced μ_h/μ_e value (3.5), while the N2200- and PNDI10-based blends showed unbalanced μ_h/μ_e values (38 and 5.8, respectively). These results suggest that the incorporation of a small amount of DCB into the N2200 main chains resulted in a balanced mobility of charge carriers in blend films, which is beneficial for charge extraction and collection. Thus, the PNDI5-based devices achieved the best FF values in all-PSCs. Moreover, a photoluminescence quenching experiment quenching experiments were performed to investigate exciton diffusion and dissociation in blend films (Fig. S9, ESI†). The
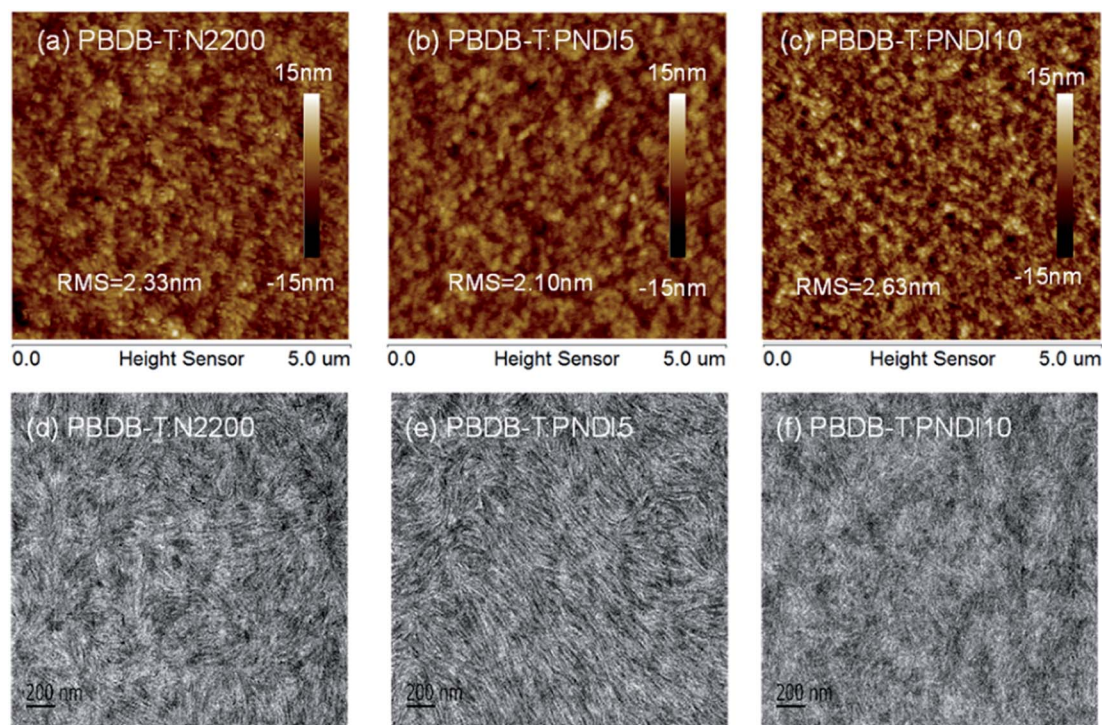

Fig. 5 AFM height images (5 × 5 μm^2) and TEM images for all-PSCs based on PBDB-T:N2200 (a and d), PBDB-T:PNDI5 (b and e), PBDB-T:PNDI10 (c and f) under optimized conditions.

quenching of the photoluminescence intensity of the PNDI5 blend films was more pronounced than the blend films of N2200 or PNDI10, indicating more efficient exciton dissociation and charge generation in the blend film with PBDB-T:PNDI5. This result is consistent with the significantly enhanced PCE of the PNDI5-based devices.

We further investigated the charge recombination behavior of all-PSCs by measuring the dependence of their J_{sc} on illumination intensity. The correlation between J_{sc} and illumination intensity (P) is quantitatively as $J_{sc} \propto (P_{light})^S$, where P_{light} is the light intensity and S is the exponential factor.[45] When the bimolecular recombination of the charge carriers is weak, J_{sc} shows a linear dependence on P_{light} with the S value almost equal to 1. The S values from the fitted line for the N2200-, PNDI5-, and PNDI10-based all-PSCs were 0.934, 0.946, 0.915, respectively (Fig. 4b), indicating that there was very weak bimolecular recombination in the device based on PBDB-T-PNDI5. The weak bimolecular recombination is associated with balanced hole and electron transport.

Film morphology

The morphological properties of optimized blend films were investigated *via* atomic force microscopy (Fig. 5a–c) and transmission electron microscopy (Fig. 5d–f). The PBDB-T:N2200 blend film exhibited granular aggregates across its surface and a root-mean-square (RMS) roughness of 2.33 nm. The PBDB-T:PNDI5 blend film formed smoother percolated fibrous structures with a slightly lower RMS roughness of 2.10 nm, suggesting that the DCB concentration of the polymer acceptor can be controlled to optimize the film morphology for charge transport (*i.e.*, enhanced hole/electron mobility) in the bulk-heterojunction films. Moreover, the transmission electron microscopy images revealed that the blend film based on PBDB-T:PNDI5 showed blurred whiskers, which are beneficial for efficient charge transport in blend films and thus contributed to the excellent FF and higher J_{sc} of the all-PSCs devices.[21]

Conclusion

We developed two terpolymer acceptors, PNDI5 and PNDI10, by introducing different numbers of DCB units into bithiophene and 2,6-dibromonaphthalene-1,4,5,8-tetracarboxylic-*N*,*N*′-bis(2-octyldodecyl)diimide. The crystallinity and nanostructures of the resulting donor–acceptor blends could be fine-tuned by adjusting the DCB concentration in the acceptor. All-PSCs based on PBDB-T:PNDI5 blend exhibited a high PCE of 8.01%, which was considerably greater than that of the device based on PBDB-T-N2200 (6.60%). The enhanced photovoltaic performances of the PBDB-T:PNDI5-based devices was due to their balanced bulk charge mobility, reduced recombination, and optimized microstructure morphology. These results indicate that the construction of terpolymer acceptors based on N2200 is a promising approach for manufacturing all-PSCs.

Conflicts of interest

The authors declare no competing financial interest.

Acknowledgements

References

1 C. Lee, S. Lee, G.-U. Kim, W. Lee and B. J. Kim, *Chem. Rev.*, 2019, **119**, 8028–8086.

2 Z. Genene, W. Mammo, E. Wang and M. R. Andersson, *Adv. Mater.*, 2019, **29**, 1807275.

3 P. Cheng and Y. Yang, *Acc. Chem. Res.*, 2020, **53**, 1218–1228.

4 J. Qin, L. Lan, S. Chen, F. Huang, H. Shi, W. Chen, H. Xia, K. Sun and C. Yang, *Adv. Funct. Mater.*, 2020, **30**, 2002529.

5 C. Zhao, J. Wang, J. Jiao, L. Huang and J. Tang, *J. Mater. Chem. C*, 2020, **8**, 28–43.

6 J. Du, K. Hu, L. Meng, I. Angunawela, J. Zhang, S. Qin, A. L.- Pelaez, C. Zhu, Z. Zhang, H. Ade and Y. Li, *Angew. Chem., Int. Ed.*, 2020, **59**, 15181–15185.

7 H. Sun, H. Yu, Y. Shi, J. Yu, Z. Peng, X. Zhang, B. Liu, J. Wang, R. Singh, J. Lee, Y. Li, Z. Wei, Q. Liao, Z. Kan, L. Ye, H. Yan, F. Gao and X. Guo, *Adv. Mater.*, 2020, **32**, 2002183.

8 Y. Zhang, Y. Xu, M. J. Ford, F. Li, J. Sun, X. Ling, Y. Wang, J. Gu, J. Yuan and W. Ma, *Adv. Energy Mater.*, 2018, **8**, 1800029.

9 N. J. Zhou, H. Lin, S. J. Lou, X. G. Yu, P. J. Guo, E. F. Manley, S. Loser, P. Hartnett, H. Huang, M. R. Wasielewski, L. X. Chen, R. P. H. Chang, A. Facchetti and T. J. Marks, *Adv. Energy Mater.*, 2014, **4**, 1300785.

10 R. H. Lee, L. C. Yang, J. Y. Wua and R. J. Jeng, *RSC Adv.*, 2017, **7**, 1016–1025.

11 W. J. Chen, Y. C. Cheng, D. W. Kuo, C. T. Chen, B. T. Liu, R. J. Jeng and R. H. Lee, *RSC Adv.*, 2018, **8**, 31478–31489.

12 D. Mori, H. Benten, I. Okada, H. Ohkita and S. Ito, *Adv. Energy Mater.*, 2014, **4**, 1301006.

13 Z. Li, L. Ying, P. Zhu, W. Zhong, N. Li, F. Liu, F. Huang and Y. Cao, *Energy Environ. Sci.*, 2019, **12**, 157–163.

14 B. Fan, W. Zhong, L. Ying, D. Zhang, M. Li, Y. Lin, R. Xia, F. Liu, H.-L. Yip, N. Li, Y. Ma, C. J. Brabec, F. Huang and Y. Cao, *Nat. Commun.*, 2019, **10**, 4100.

15 B. Xie, K. Zhang, Z. Hu, H. Fang, B. Lin, Q. Yin, B. He, S. Dong, L. Ying, W. Ma, F. Huang, H. Yan and Y. Cao, *Sol. RRL*, 2019, **4**, 1900385.

16 N. B. Kolhe, D. K. Tran, H. Lee, D. Kuzuhara, N. Yoshimoto, T. Koganezawa and S. A. Jenekhe, *ACS Energy Lett.*, 2019, **4**, 1162–1170.

17 Y. Guo, Y. Li, O. Awartani, H. Han, J. Zhao, H. Ade, H. Yan and D. Zhao, *Adv. Mater.*, 2017, **29**, 1700309.

18 S. Li, H. Zhang, W. Zhao, L. Ye, H. Yao, B. Yang, S. Zhang and J. Hou, *Adv. Energy Mater.*, 2016, **6**, 1501991.

19 X. Long, Z. Ding, C. Dou, J. Zhang, J. Liu and L. Wang, *Adv. Mater.*, 2016, **28**, 6504–6508.

20 R. Zhao, N. Wang, Y. Yu and J. Liu, *Chem. Mater.*, 2020, **32**, 1308–1314.

21 Z.-G. Zhang, Y. Yang, J. Yao, L. Xue, S. Chen, X. Li, W. Morrison, C. Yang and Y. Li, *Angew. Chem., Int. Ed.*, 2017, **56**, 13503–13507.

22 H. Yao, F. Bai, H. Hu, L. Arunagiri, J. Zhang, Y. Chen, H. Yu, S. Chen, T. Liu, J. Y. L. Lai, Y. Zou, H. Ade and H. Yan, *ACS Energy Lett.*, 2019, **4**, 417–422.

23 J. Wu, Y. Meng, X. Guo, L. Zhu, F. Liu and M. Zhang, *J. Mater. Chem. A*, 2019, **7**, 16190–16196.

24 H. Sun, Y. Tang, C. W. Koh, S. Ling, R. Wang, K. Yang, J. Yu, Y. Shi, Y. Wang, H. Y. Woo and X. Guo, *Adv. Mater.*, 2019, **31**, 1807220.

25 T. Jia, J. Zhang, W. Zhong, Y. Liang, K. Zhang, S. Dong, L. Ying, F. Liu, X. Wang, F. Huang and Y. Cao, *Nano Energy*, 2020, **72**, 104718.

26 W. Wang, Q. Wu, R. Sun, J. Guo, Y. Wu, M. Shi, W. Yang, H. Li and J. Min, *Joule*, 2020, **4**, 1070–1086.

27 Z. Luo, T. Liu, R. Ma, Y. Xiao, L. Zhan, G. Zhang, H. Sun, F. Ni, G. Chai, J. Wang, C. Zhong, Y. Zou, X. Guo, X. Lu, H. Chen, H. Yan and C. Yang, *Adv. Mater.*, 2020, **30**, 2005942.

28 A. Tang, J. Li, B. Zhang, J. Peng and E. Zhou, *ACS Macro Lett.*, 2020, **9**, 706–712.

29 Q. Fan, Q. An, Y. Lin, Y. Xia, Q. Li, M. Zhang, W. Su, W. Peng, C. Zhang, F. Liu, L. Hou, W. Zhu, D. Yu, M. Xiao, E. Moons, F. Zhang, T. D. Anthopoulos, O. Inganäs and E. Wang, *Energy Environ. Sci.*, 2020, **13**, 5017–5027.

30 H. Yan, Z. Chen, Y. Zheng, C. Newman, J. R. Quinn, F. Dotz, M. Kastler and A. Facchetti, *Nature*, 2009, **457**, 679.

31 C. Mu, P. Liu, W. Ma, K. Jiang, J. Zhao, K. Zhang, Z. Chen, Z. Wei, Y. Yi, J. Wang, S. Yang, F. Huang, A. Facchetti, H. Ade and H. Yan, *Adv. Mater.*, 2014, **26**, 7224.

32 J. W. Jung, J. W. Jo, C. C. Chueh, F. Liu, W. H. Jo, T. P. Russell and A. K. Jen, *Adv. Mater.*, 2015, **27**, 3310.

33 L. Zhu, W. Zhong, C. Qiu, B. Lyu, Z. Zhou, M. Zhang, J. Song, J. Xu, J. Wang, J. Ali, W. Feng, Z. Shi, X. Gu, L. Ying, Y. Zhang and F. Liu, *Adv. Mater.*, 2019, **31**, 1902899.

34 Z. Li, X. Xu, W. Zhang, X. Meng, W. Ma, A. Yartsev, O. Inganas, M. R. Andersson, R. A. Janssen and E. Wang, *J. Am. Chem. Soc.*, 2016, **138**, 10935–10944.

35 X. Liu, C. Zhang, C. Duan, M. Li, Z. Hu, J. Wang, F. Liu, N. Li, C. J. Brabec, R. A. J. Janssen, G. C. Bazan, F. Huang and Y. Cao, *J. Am. Chem. Soc.*, 2018, **140**, 8934–8943.

36 D. Chen, J. Yao, L. Chen, J. Yin, R. Lv, B. Huang, S. Liu, Z.-G. Zhang, C. Yang, Y. Chen and Y. Li, *Angew. Chem., Int. Ed.*, 2018, **57**, 1–6.

37 J.-W. Lee, M. Sung, D. Kim, S. Lee, H. You, F. S. Kim, Y.-H. Kim, B. J. Kim and S.-K. Kwon, *Chem. Mater.*, 2020, **32**, 2572–2582.

38 B. He, Q. Yin, X. Yang, L. Liu, X.-F. Jiang, J. Zhang, F. Huang and Y. Cao, *J. Mater. Chem. C*, 2017, **5**, 8774–8781.

39 B. He, Q. Yin, J. Zhang, T. Jia, X. Yang, X.-F. Jiang, F. Huang and Y. Cao, *Chin. J. Chem.*, 2018, **36**, 406.

40 R. Steyrleuthner, R. Di Pietro, B. A. Collins, F. Polzer, S. Himmelberger, M. Schubert, Z. Chen, S. Zhang, A. Salleo, H. Ade, A. Facchetti and D. Neher, *J. Am. Chem. Soc.*, 2014, **136**, 4245–4256.

41 Z. Hu, L. Ying, F. Huang and Y. Cao, *Sci. China: Chem.*, 2017, **60**, 571–582.

42 Y. Zhang, Y. Xu, M. J. Ford, F. Li, J. Sun, X. Ling, Y. Wang, J. Gu, J. Yuan and W. Ma, *Adv. Energy Mater.*, 2018, **8**, 1800029.

43 B. Fan, L. Ying, Z. Wang, B. He, X.-F. Jiang, F. Huang and Y. Cao, *Energy Environ. Sci.*, 2017, **10**, 1243–1251.

44 J.-L. Wu, F.-C. Chen, Y.-S. Hsiao, F.-C. Chien, P. Chen, C.-H. Kuo, M. H. Huang and C.-S. Hsu, *ACS Nano*, 2011, **5**, 959–967.

45 M. M. Mandoc, F. B. Kooistra, J. C. Hummelen, B. de Boer and P. W. M. Blom, *Appl. Phys. Lett.*, 2007, **91**, 263505.